Atomic layer deposition of lithium phosphates as solid-state electrolytes for all-solid-state microbatteries



2014 Nanotechnology 25 504007

(http://iopscience.iop.org/0957-4484/25/50/504007)

IOP Publishing Nanotechnology
Nanotechnology **25** (2014) 504007 (8pp) doi:10.1088/0957-4484/25/50/504007

# Atomic layer deposition of lithium phosphates as solid-state electrolytes for all-solid-state microbatteries

**Biqiong Wang[1,2], Jian Liu[1], Qian Sun[1], Ruying Li[1], Tsun-Kong Sham[2,3] and Xueliang Sun[1,3]**

[1] Department of Mechanical and Materials Engineering, University of Western Ontario, London, ON, N6A 5B9, Canada
[2] Department of Chemistry, University of Western Ontario, London, ON, N6A 5B7, Canada

E-mail: tsham@uwo.ca and xsun@eng.uwo.ca

Received 2 July 2014, revised 1 September 2014
Accepted for publication 15 September 2014
Published 28 November 2014

**Abstract**

Atomic layer deposition (ALD) has been shown as a powerful technique to build three-dimensional (3D) all-solid-state microbattery, because of its unique advantages in fabricating uniform and pinhole-free thin films in 3D structures. The development of solid-state electrolyte by ALD is a crucial step to achieve the fabrication of 3D all-solid-state microbattery by ALD. In this work, lithium phosphate solid-state electrolytes were grown by ALD at four different temperatures (250, 275, 300, and 325 °C) using two precursors (lithium tert-butoxide and trimethylphosphate). A linear dependence of film thickness on ALD cycle number was observed and uniform growth was achieved at all four temperatures. The growth rate was 0.57, 0.66, 0.69, and 0.72 Å/cycle at deposition temperatures of 250, 275, 300, and 325 °C, respectively. Furthermore, x-ray photoelectron spectroscopy confirmed the compositions and chemical structures of lithium phosphates deposited by ALD. Moreover, the lithium phosphate thin films deposited at 300 °C presented the highest ionic conductivity of $1.73 \times 10^{-8}$ S cm$^{-1}$ at 323 K with ~0.51 eV activation energy based on the electrochemical impedance spectroscopy. The ionic conductivity was calculated to be $3.3 \times 10^{-8}$ S cm$^{-1}$ at 26 °C (299 K).

Keywords: atomic layer deposition, solid-state electrolyte, lithium phosphate

(Some figures may appear in colour only in the online journal)

## 1. Introduction

Microelectronic devices play a continuously and increasingly indispensible role in our daily life, such as medical implants, micro sensors, and microelectromechanical systems. The continually downscaling of the products requires the on-board power supply device to be of smaller dimensions, higher energy and power density [1]. Microbattery is the preferable energy devices for such applications. In particular, the all-solid state lithium-ion microbattery has been of continuous interest as an efficient energy storage system [2, 3]. Comparing to liquid-electrolyte-based microbatteries, all-solid-state microbatteries offer several advantages. First, more flexibility is provided in battery design and management. Secondly, miniaturized size extends the applications on microelectronic devices. Thirdly and more importantly, the inherent problems coming with liquid electrolytes including the release of heat during cycling, inflammability of the electrolyte, and the potential leakage could all lead to severe safety hazards. Some significant issues plaguing the development of batteries such as the degradation effect and the safety problem can be expected to be well resolved through all-solid-state microbatteries [4, 5].

During the past decade, great effort has been devoted to developing two-dimensional (2D) thin film all-solid-state micro lithium ion batteries (micro-LIBs) [5–8]. A typical thin film all-solid-state LIB, which has similar structure as commercial LIBs, is composed of thin film positive electrode (e.g.

[3] Authors to whom any correspondence should be addressed.

 

$LiCoO_2$ [4, 5]), solid-state electrolyte (e.g. nitrogen-doped lithium phosphate (LIPON) [7, 8]) and negative electrode (e.g. metallic lithium [5] and $TiO_2$ [6]). Among these components, the thin film solid-state electrolytes play the most critical roles. Different techniques have been developed to deposit thin film solid-state electrolytes, including radio frequency (RF) magnetron sputtering [8], chemical vapor deposition (CVD) [7], pulsed layer deposition [9], and atomic layer deposition (ALD) [10].

However, the miniaturization of power sources and demands on high power and energy density expose the limitations of such designs [11]. The three-dimension (3D) microbatteries are desirable to achieve higher performance. A most significant advantage of 3D microbatteries over 2D thin film batteries is that it has much higher specific surface area which provides higher energy density while it keeps short diffusion path, giving better power density [12, 13]. The challenges in fabricating 3D microbatteries mainly lie in the narrow battery assemblies, implying rather complicated designs in small footprint architecture [14]. Conventional techniques for depositing thin films such as RF sputtering or CVD are not suitable in such delicate 3D structures below micro scale. Problems include non-uniform deposition, failure of interface because of cracking or roughness of the surface, giving rise to short circuit and failure of batteries [15].

ALD stands out from all the other approaches in depositing conformal and pin-hole free thin films on 3D high-aspect-ratio substrates [16]. ALD is a vapor-phase deposition process, and the precursors are pulsed into the reaction chamber in sequence and the growth of the thin films are dictated by the self-terminating gas–solid surface reactions [16]. With film growth taking place in a cyclic manner, the saturation reaction conditions gives a self-limiting growth mechanism, which offers exquisite thickness control at atomic level and adjustable stoichiometric composition. Given a large area for deposition, the process is easy to scale up with high conformity and reproducibility [17]. Substrates of high aspect ratio can also be applied because of the excellent step coverage and the growth of the film, which is independent of the geometry due to the nature of the gas phase precursors in ALD processes [18–21]. The aforementioned advantages make ALD the unique method to fabricate thin film electrolyte for 3D microbatteries. Cheah *et al* [22] reported that a nanostructured 3D $TiO_2$ electrode prepared by ALD exhibited ten times higher areal capacity than the 2D counterpart. Another group used biological scaffolds of high aspect ratio as substrates and synthesized $Ni/TiO_2$ nanocomposite anodes via ALD. The $Ni/TiO_2$ electrodes presented excellent capacity and rate capability, and extremely low capacity fading [23]. More recently, ALD (depositing $V_2O_5$ as cathodes) combined with micromachining was applied in 3D microbatteries. The hierarchical 3D micro- and nanostructured electrodes exhibited three-fold increase in energy density compared with nanosturctures alone due to the enlarged surface area [24].

Even though no full 3D all-solid-state micro-LIBs has been manufactured by ALD yet, the application of ALD in fabricating key battery components (the anode, cathode, and solid-state electrolyte) has been intensively investigated. Recently, a few cases of anode (such as $SnO_2$, $TiO_2$) [22, 25–27] and cathode (like $V_2O_5$, $LiCoO_2$) [28, 29] materials of LIBs has been successfully developed. Another crucial component in all-solid-state LIBs is solid-state electrolyte. Available materials containing lithium have been developed. Recently it was reported the successful synthesis of $Li_2O$ by Aaltonen *et al* [30], which promoted the rapid progress in the study of solid-state electrolytes derived by ALD. Aaltonen *et al* [31] grew lithium lanthanum titanate from lithium turtbutoxide, $TiCl_4$, $La(thd)_3$ (thd = 2,2,6,6-tetramethyl-3,5-heptanedione)), ozone, and water. Later on, $Li_2O$–$Al_2O_3$ ($LiAlO_x$) was prepared by combining ALD subcycles of $Li_2O$ and $Al_2O_3$ using lithium tert-butoxide, TMA and water as precursors [32, 33]. This material was lately used as a coating material for increased interracial stability in high voltage LIBs [34]. Other lithium containing compounds include lithium silicate [35], lithium niobate [36], lithium tantalate [10], lithium nitride [37], and $Li_xAl_ySi_zO$ [38].

In order to be employed in all-solid-state microbatteries, ionic conductivity is an important parameter for solid-state electrolytes, but was seldom reported in previous studies. The lithium-ion conductivity could reach $1 \times 10^{-7}$ S cm$^{-1}$ at 300 °C for $Li_2O$–$Al_2O_3$ after being annealed at 700 °C for 5 h [33]. However, the drastic post heat treatment could cause severe damage to electrode materials or problems like cracking could occur when the solid-state electrolyte is used in LIBs, which is fatal to the battery system. Therefore, it is an approachable strategy to explore materials with high ionic conductivity without post-annealing treatment using ALD. Moreover, an easy ALD process is more favorable for the real application in 3D microbatteries.

Apart from the above materials, $Li_3PO_4$ has proved to be a promising candidate as solid-state electrolyte due to its good ionic conductivity of $7 \times 10^{-8}$ S cm$^{-1}$ at 25 °C in amorphous thin film structures [39]. Furthermore, it is clearly evident that amorphous $Li_3PO_4$ exhibits a higher ionic conductivity ($6.6 \times 10^{-8}$ S cm$^{-1}$ at 25 °C) than its crystalline counterpart ($4.2 \times 10^{-18}$ S cm$^{-1}$ at 25 °C) [39, 40]. This implies that the film prepared by the relatively mild ALD process has a lower risk of fracturing and can be readily employed in LIB either as solid-state electrolyte. Hämäläinen *et al* established a thorough ALD process for synthesizing $Li_3PO_4$, which contains two precursors (lithium tert-butoxide and trimethylphosphate) avoiding the complication of ALD sub cycles when applied in 3D microbatteries. However, no electrochemical results were shown in this work [41]. Herein, we carry out the ALD process of $Li_3PO_4$, and optimize the ALD process in terms of the electrochemical performance of the $Li_3PO_4$ thin film electrolytes. The lithium phosphate thin films produced by ALD are featured with not only extremely conformal and uniform deposition with well-tuned composition, but also moderate lithium ion conductivity in the order of $10^{-7}$ S cm$^{-1}$ at 50 °C, without any additional post treatment process. In summary, lithium phosphate deposited by ALD is an ideal candidate as thin film electrolyte in 3D all-solid-state micro-LIBs.

## 2. Experimental

All the lithium phosphate thin films were grown on silicon (100) or glass substrates in a Savannah 100 ALD system (Cambridge Nanotech). Lithium tert-butoxide [LiO$^t$Bu, $(CH_3)_3COLi$] was used as lithium source and trimethylphosphate [TMPO, $(MeO)_3PO$] as phosphate source. The source temperature for LiO$^t$Bu and TMPO was 180 and 75 °C, respectively. The system pipelines were maintained at 190 °C in order to prevent the condensation of the precursors. The lithium phosphates were deposited at four different temperatures, i.e. 250, 275, 300, and 325 °C. LiO$^t$Bu and TMPO were pulsed into the chamber alternatively with the same pulse time duration separated by a 15 s nitrogen purge. Different pulse times of 1, 2, and 4 s were used. Morphology, structure, and composition characterizations were conducted on lithium phosphate films deposited on the Si(100) substrates, while electrochemical impedance characterization was carried out on lithium phosphate film on Au-coated glass.

Film thicknesses were measured from the fresh-cut cross-sections using field-emission scanning electron microscopy (Hitachi-4800). Five different spots of each film were randomly selected and the average thickness was taken to obtain the final thickness. The compositions of the lithium phosphates were determined by x-ray photoelectron spectroscopy (XPS) using a Kratos Axis Ultra Al (alpha) spectrometer.

The depth distribution of the elements in the films was studied by secondary ion mass spectrometry (SIMS) using a Cameca IMS-6f ion microprobe. An area of $250 \times 250\ mm^2$ was sputtered by a negative oxygen beam. The depth scales were obtained by measuring the SIMS craters with a Tencor P-10 surface profilometer.

Electrochemical impedance spectra (EIS) of the lithium phosphate thin film on glass were evaluated on a CHI electrochemistry workstation in a frequency range of 200 kHz–100 Hz. A sandwich structure of Au-thin film electrolyte-Au on glass substrate was designed for the EIS measurements. Au layers were deposited by sputtering. The sputtering processes were carried out in a Polaron sputtering system under 2 kV for 9 min with a current of 25 mA, to achieve a thickness of $50 \pm 5$ nm of Au. The thickness of lithium phosphate thin film was $130 \pm 10$ nm. The geometric areas of the thin film electrolytes between the two Au electrodes were $4\ mm \times 4\ mm$. Temperature was elevated from 323 K to 403 K (10 K step) and the samples were maintained at each temperature for 20 min for stabilization before acquiring the spectra.

## 3. Results and discussion

Lithium phosphate thin films grown using 2000 ALD cycles at 250 °C (LPO250), 275 °C (LPO275), 300 °C (LPO300), and 325 °C (LPO325) have been examined by SEM, and the results are displayed in figure 1. From the cross-section views in figure 1, it can be seen that the lithium phosphate film is uniformly deposited on the Si substrate at all the deposition temperatures, giving an ultra flat surface on the substrate. The thicknesses of LPO250, LPO275, LPO300, and LPO325 are measured to be 112, 133, 137, and 154 nm, respectively. Figure 2 displays the film thickness of lithium phosphate film as a function of ALD cycle number at each deposition temperature. It is obvious that the film thickness of lithium phosphate is linearly proportional to the number of ALD cycles, indicating the self-limiting behavior of the ALD process. After fitting the data in figure 2, the growth per cycle of lithium phosphate film is calculated to be 0.57, 0.66, 0.69, and 0.74 Å/cycle at the deposition temperatures of 250, 275, 300, and 325 °C, respectively. The deposition temperature dependence of the growth rates was plotted in figure 2(b), from which one can see that the film is deposited faster at elevated temperatures, in accordance with the literatures [41, 42]. The reason could be that higher temperature promotes the ligands exchange process in the ALD process. The reactivity between LiO$^t$Bu and TMPO is higher at elevated temperature. More reactions lead to higher growth rate. The growth rates of lithium phosphate in this work are lower than the reported ones (0.7–1 Å/cycle) in the similar temperature range (225–300 °C). In our work, LPO250 and LPO300 have a growth rate of 0.57 and 0.74 Å/cycle, respectively, while it was reported 0.7 and 1 Å/cycle at the same temperatures [41]. It can be explained by the less pulse time (2 s) of both of the precursors (LiO$^t$Bu and TMPO) applied in our work. Shorter (1 s) and longer pulse time (4 s) were used at 300 °C and the growth rate was shown in figure 2(b). With 4 s of pulse time, the growth rate reaches 0.94 Å/cycle. In addition, the growth rate with 2 s of pulse time is also in accordance with the reported one [41]. The growth rate increased with the pulse time of LiO$^t$Bu. No full saturation was observed with 4 s of pulse time. The reason is that this system is not an ideal ALD process. No normal oxidizer like $H_2O$, $O_2$, and $O_3$ was used. More ligands exchange occurs when exposed to the reactants for longer time, providing larger growth rate. The decomposition of LiO$^t$Bu is reported to take place at 350 °C [41]. When the temperature reached 325 °C, a slight color change observed in the deposition chamber indicates that there might be a degree of decomposition of LiO$^t$Bu. Therefore, LPO325 was not further tested in the following electrochemical measurements.

XPS measurements were carried out in order to determine the chemical composition of the ALD deposited lithium phosphate thin films, and the results are presented in figure 3. The XPS survey in figure 3(a) shows that lithium phosphate thin films contain Li, P, C, and O elements (the atomic percentages listed in table SI-1). For LPO250 and LPO300, the atomic ratio of Li to P elements is calculated to be 3.33 and 2.80 respectively, which are close to that of standard $Li_3PO_4$. In the slow scan of Li 1s shown in figure 3(b), the peak position of Li 1s locates at ~55.26 eV, which corresponds well to that of standard $Li_3PO_4$ [43]. There is no observable shift in Li 1s for $Li_{2.80}PO_z$ and $Li_{3.33}PO_z$ (55.26 eV for $Li_{2.80}PO_z$ and 55.52 eV for $Li_{3.33}PO_z$), indicating the single chemical environment of Li (Li–O) in both of the lithium phosphate thin films. The P 2p spectra can be fitted into a set of doublet P $2p_{1/2}$ and P $2p_{3/2}$, which are centered at about 134.04 and 133.20 eV, respectively. No evident shift is

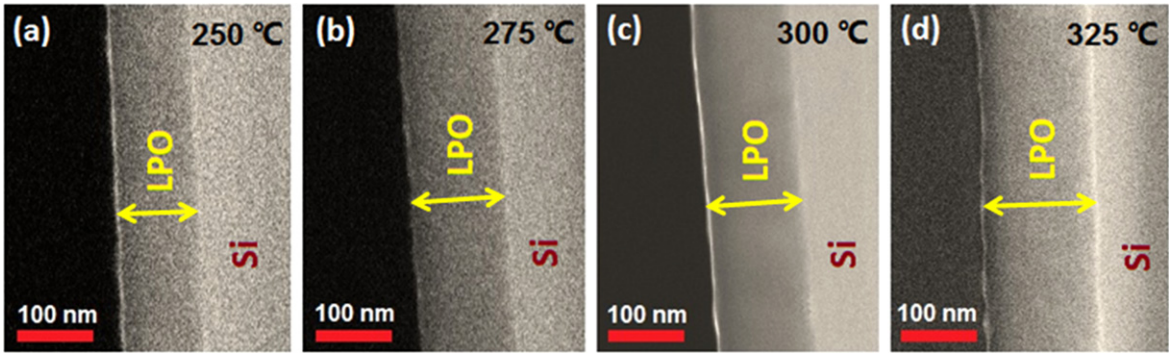


**Figure 1.** Cross-section SEM pictures of the ALD deposited lithium phosphate thin films on Si(100) substrates at (a) 250 °C (LPO250), (b) 275 °C (LPO275), (c) 300 °C (LPO300), and (d) 325 °C (LPO325), after 2000 ALD cycles.

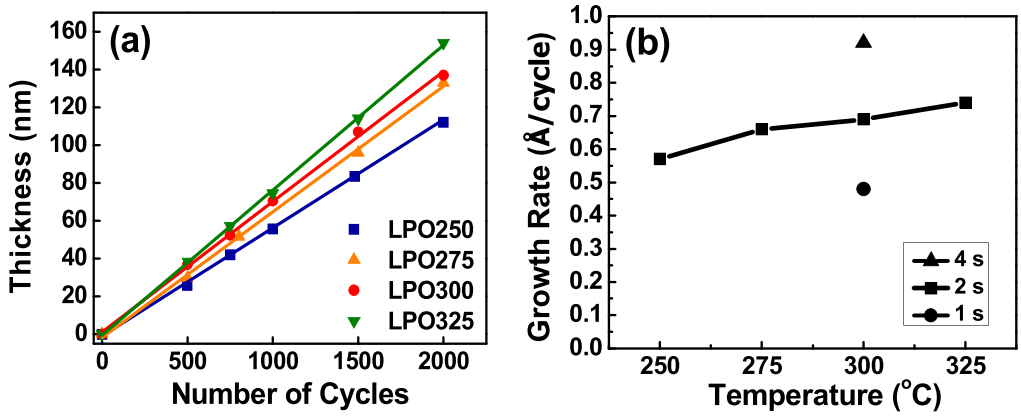


**Figure 2.** (a) Thickness of the lithium phosphate thin films as a function of the number of ALD cycles; (b) the thin film growth rates as a function of deposition temperature.

observed between the spectra of LPO250 and LPO300. Assigning the P 2p in phosphate in reference to the standard spectra of $Li_3PO_4$ (2p peak at 133.2 eV) [43], the result reveals that P in the lithium phosphate films shares a similar chemical state as that in standard $Li_3PO_4$. Furthermore, deconvolution of O 1s peak in figure 3(d) consists of two components located at 532.69 eV and 531.25 eV for both LPO250 and LPO300. The former belongs to the oxygen in organics at higher binding energy (532.69 eV), and the latter corresponds to the oxygen in phosphates, which is consistent with the conclusion from the spectra of P 2p and agrees with the standard O peaks of $Li_3PO_4$ (at 531.1 eV) [43]. Also, carbon is detected in all thin films prepared (figure 3(a)). The carbon detected on the surface exists in forms of O–C=O (288.80 eV), C=O (287.80 eV), C–OH, C–O–C (286.30 eV), and C–C, C–H (284.80 eV) in both C 1s spectra of LPO250 and LPO300. Besides, a trace of carbonate (290.04 eV) was found in LPO250 (see figure SI-1). The organic carbon might be resulted from the residual ligands from ALD precursors, which could not be efficiently removed by purging and is commonly observed in XPS. The source of the carbonate is the reaction between $Li_2O$ in the lithium-containing films and $CO_2$ when the thin films are exposed to ambient air [33]. The reason that carbonate is only detectable in LPO250 rather than LPO300 can be due to the higher content of lithium on the surface (see figure SI-3), which reacts with ambient carbon dioxide more readily. Therefore, it can be concluded that lithium phosphate prepared by ALD has similar chemical structure as standard $Li_3PO_4$.

Lithium-ion conductivities of the lithium phosphate thin films LPO250, LPO275, and LPO300 were measured using electrochemical impedance spectroscopy. Figure 4 displays the Cole–Cole plots obtained at temperatures between 323 and 403 K and the Arrhenius plot of the ionic conductivities of the deposited thin films.

The complex impedance plots in figures 4(a) and (b) are composed of one semicircle in the high-frequency region and one linear tail at lower frequency. The semicircle is addressed to the bulk resistance of lithium phosphate solid-state electrolytes, while the linear tail is due to the polarization at electrode–electrolyte interface [10]. The insets depict the equivalent circuits used to resolve the Cole–Cole plots, where $R_0$ denotes the high-frequency limiting resistance of the electrodes, and $R_b$ represents for the bulk resistance. CPE stands for constant-phase element. A CPE is commonly used in a model in place of a capacitor, considered to be the resultant bulk capacitance of the lithium phosphate solid-state electrolyte. $W$ in the circuit is the finite length Warburg element, which occurs when charge carrier diffuses through the solids [44]. In this case, lithium ion is the charge carrier. Since Au applied as the electrode material is ionic blocking (open circuit diffusion), the behavior thus observed is typical of an

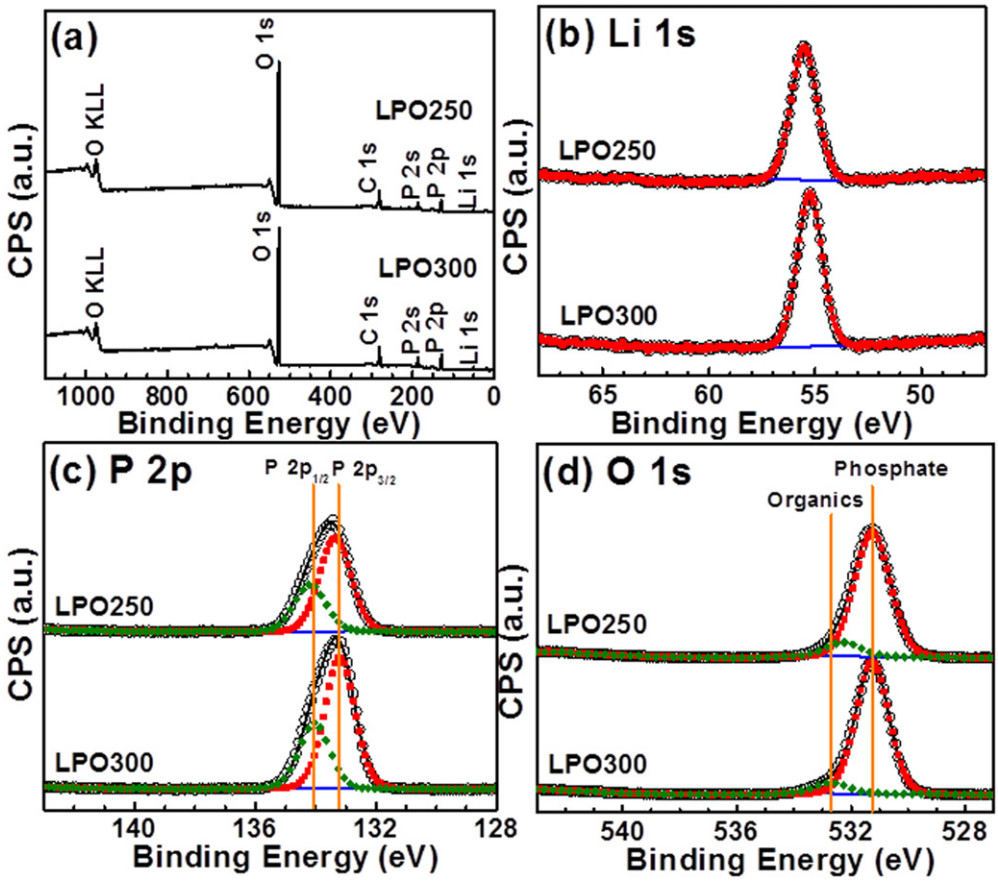


**Figure 3.** (a) XPS survey of the lithium phosphate thin films LPO250 and LPO 300 deposited on Si (100); deconvolution of (b) Li 1s (c) P 2p and (d) O 1s spectra.

ionic conductor in nature [44]. The ionic conductivity of the lithium phosphate thin films was evaluated by substituting the empirical $R_b$ values into the equation below [10]:

$$\sigma = d/(AR_b), \tag{1}$$

where $\sigma$ is the ionic conductivity, $d$ is the thickness of the lithium phosphate thin film, and $A$ is the geometric area of the lithium phosphate thin film between the Au electrodes. Thin film LPO250 yields a resistance from 387.8 $\Omega$ to 381.2 k$\Omega$, giving conductivity from $3.72 \times 10^{-10}$ to $3.79 \times 10^{-7}$ S cm$^{-1}$, at measuring temperatures between 323 and 403 K. From figure 4(b), the resistance of LPO275 acquired within the same measuring temperature range (323–403 K) varies from 17 854 $\Omega$ to 241.4 k$\Omega$ and thus its ionic conductivity falls between $6.85 \times 10^{-10}$ and $5.06 \times 10^{-7}$ S cm$^{-1}$.

For the lithium phosphate film deposited at 300 °C, figure 4(c) shows only complete symmetric semicircular arcs indicative of a parallel *R*–*C* network (figure 4(c) inset) and no diffusion element is present at the lower frequency end [45, 46]. No diffusion effects appear when only charge of a single sign is mobile (lithium ions of positive charge); this is an excellent approximation of solid-state electrolytes [44]. The resistance in this figure reaches 0.47 k$\Omega$ even at 323 K and drops to 0.014 k$\Omega$ at 403 K. Therefore the calculated ionic conductivity of LPO300 is as high as $1.72 \times 10^{-7}$ S cm$^{-1}$ at 323 K and $4.50 \times 10^{-5}$ S cm$^{-1}$ at 403 K. These values are three orders higher than those of LPO250 and LPO275. Therefore, it is found that the increasing deposition temperature (within 250–300 °C) in the ALD process provides higher ionic conductivity of lithium phosphate solid-state electrolyte.

Furthermore, the activation energies of the thin film electrolytes are calculated by plotting Ln ($\sigma T$) against 1000/$T$ according to the Arrhenius equation [46]:

$$\sigma T = A \exp\left[-E_a/(kT)\right], \tag{2}$$

where $T$ is the absolute temperature, $A$ is a pre-exponential factor, $E_a$ is the activation energy, and $k$ represents the Boltzmann constant. The value of activation energy can be extracted by linearly fitting the results in a ln plot. Figure 4(d) demonstrates that $E_a$ of the lithium phosphate thin films LPO250, LPO275, and LPO300 are of ~1.02, ~0.93, and ~0.51 eV, respectively. Comparing the conductivities of lithium phosphate solid-state electrolytes prepared by ALD at 250, 275, and 300 °C, it is found that ionic conductivity is reliant on deposition temperature. Higher temperature results in improved ionic conductivity in the ALD deposited lithium phosphate thin film system in this study. Referring to the previous studies, in this amorphous oxides system, when the ratio of Li to P is 1, metaphosphate structural units (SUs) are formed. SUs consist of oxygen tetrahedral [$PO_4$] connected in chains by bridging oxygen atoms. Tie chains are formed

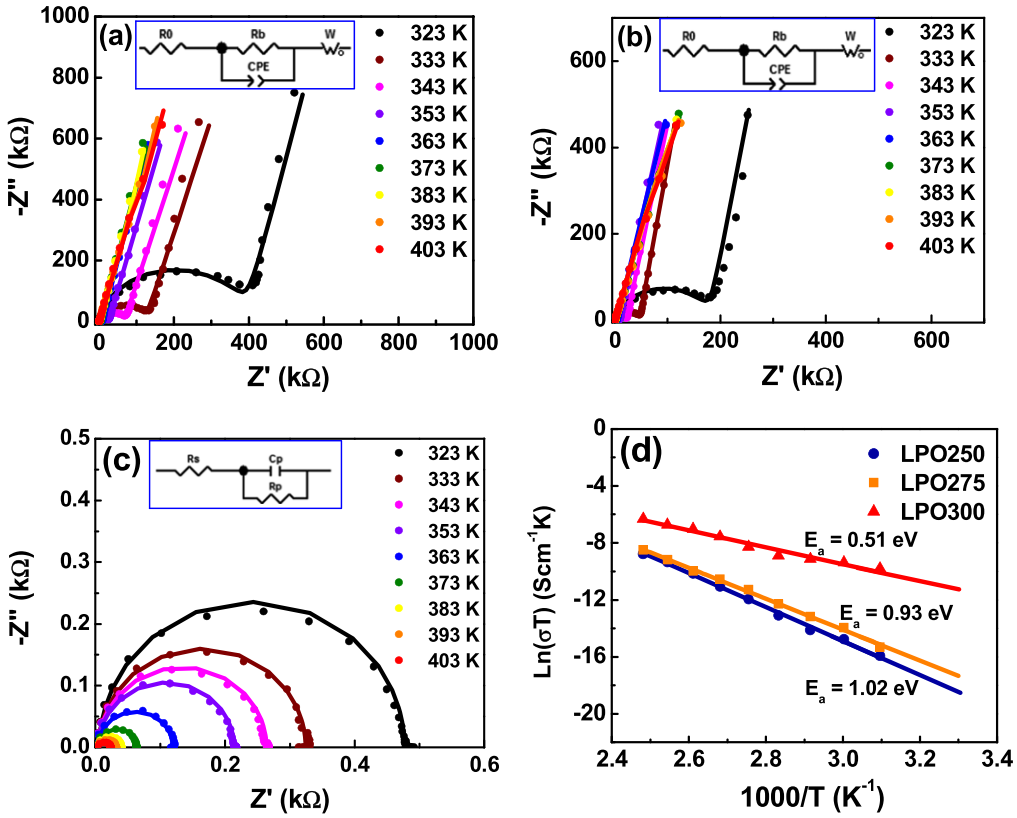


**Figure 4.** Impedance plots of lithium phosphate thin films (a) LPO250, (b) LPO275, and (c) LPO300 measured at different temperatures (insets are the equivalent circuits employed for simulation); (d) Arrhenius plots of the ionic conductivity of the lithium phosphate films measured between 323 and 403 K. (Scattered points are measured value and lines are fitted results.)

between SUs threading the entire volume. The ionic conductivity is related to the migration of lithium ions in the thin films. The oxygen shared by SUs are negatively charged and lithium ions are dissociated from the polar structural chemical units, hopping from one to another to achieve the migration [47]. Another factor is the lithium concentration in the thin films. As the current carrier, introducing more lithium content can efficiently improve the ionic conductivity [45, 47]. In this study, LPO250 has a higher Li to P ratio but a much lower ionic conductivity compared to LPO300. Therefore, it could be explained that the former factor is dominant. Higher deposition temperature could lead to growth of number of terminal oxygen atoms and formation of shorter-chain SUs. In addition, the polarization of the structural chemical units is of higher degree, resulting in decreasing the tightness of fixation of lithium ions in the structure, which is beneficial to the mobility of lithium ions. Hence the ionic conductivity is improved owing to a drop in the activation energy of conductivity [45, 47].

Extrapolation of the lines in figure 4(d) reads an ionic conductivity of $3.3 \times 10^{-8}$ S cm$^{-1}$ at RT, for thin film LPO300. This result is superior than those of other ALD deposited solid-state electrolytes. For example, the ionic conductivity of $Li_2O$–$Al_2O_3$ was reported to be $1 \times 10^{-7}$ S cm$^{-1}$ at 573 K, with a rather high activation energy of 2.90 eV. At RT, the conductivity would drop dramatically. Besides, the as-prepared $Li_2O$–$Al_2O_3$ electrolyte had to be annealed at 700 °C prior to the measurement [33]. The post-treatment could be detrimental when applied to real battery fabrication. The ultrathin coatings of $Li_{5.1}TaO_z$ and $LiAlO_2$ were applied to cathode materials of LIBs, exhibiting similar ionic conductivities to this work [34, 48]. Nonetheless, the ALD processes of preparing the $Li_{5.1}TaO_z$ and $LiAlO_2$ thin films employs water as a precursor. The little trace of residue of water could be hazardous to battery performance. This work conducted here is a water-free ALD process. Another system successfully synthesized is $Li_xAl_ySi_zO$ [38]. Despite the fairly good ionic conductivity, the rather complicated ALD process combines the subcycles of three oxides (four precursors) comparing to lithium phosphate thin films which only needs two precursors to set off .

Overall, we managed to achieve thin film lithium phosphate electrolyte with an acceptable ionic conductivity via a much simplified ALD process. Its electrochemical property is either comparable to or better than the lithium phosphate films fabricated by other reported methods such as RF sputtering and solid state reaction [39, 40] which is summarized in table 1. Moreover, the ALD process is able to produce the films with ultra thin thickness, extreme uniformity, and application to micro-3D structures. Lithium phosphate solid-state electrolyte deposited by ALD can be of great potential in both the application of all-solid-state micro-LIBs in future and as beneficial coating layers on the electrodes for LIBs.

**Table 1.** Comparisons of lithium phosphates deposited by ALD and conventional methods.

| Solid-State electrolyte | Substrate | $Li^+$ conductivity (S $cm^{-1}$) | Activation energy (eV) | Method | References |
|---|---|---|---|---|---|
| $Li_{2.8}PO_z$ | Si (100)/glass | $3.3 \times 10^{-8}$ (at 299 K) | 0.51 | ALD | This work |
| $Li_{2.7}PO_{3.9}$ | Sapphire/graphite/alumina/glass | $6.6 \times 10^{-8}$ (at 298 K) | 0.68 | RF sputtering | [39] |
| Polycrystallin $\gamma$-$Li_3PO_4$ | — | $4.2 \times 10^{-18}$ (at 298 K) | 1.24 | Solid state reaction | [40] |

## 4. Conclusion

In summary, lithium phosphate thin films were deposited at 250, 275, 300, and 325 °C by ALD using $LiO^tBu$ and TMPO as precursors, without any additional oxidizer. Self-limiting growths of lithium phosphate thin film were achieved at all the temperatures. The growth rate of lithium phosphate thin films was 0.57, 0.66, 0.69, and 0.74 Å/cycle at 250, 275, 300, and 325 °C, respectively. XPS analysis showed that the as-deposited films had similar chemical structure as that in standard $Li_3PO_4$, and a higher deposition temperature provided a lower Li to P and O to P ratio. Furthermore, the lithium-ion conductivities of the films were measured. Lithium phosphate films grown at 300 °C exhibited the highest ionic conductivity of $1.73 \times 10^{-7}$ S $cm^{-1}$ at 323 K with an activation energy of 0.51 eV. The extrapolated ionic conductivity at RT was $3.3 \times 10^{-8}$ S $cm^{-1}$. It is expected that the lithium phosphate thin films prepared by ALD can find potential applications as solid-state electrolytes for 3D all-solid-state micro-LIBs, which, as an emerging area, deserves more extensive investigation in the coming future.

## Acknowledgment

This work was supported by Nature Sciences and Engineering Research Council of Canada (NSERC), Canada Research Chair (CRC) Program, Canada Foundation for Innovation (CFI), the Canada Light Source (CLS) at University of Saskatchewan, and University of Western Ontario.

## References

[1] Roberts M *et al* 2011 3D lithium ion batteries—from fundamentals to fabrication *J. Mater. Chem.* **21** 9876–90
[2] Goodenough J B and Park K-S 2013 The Li-ion rechargeable battery: a perspective *J. Am. Chem. Soc.* **135** 1167–76
[3] Goodenough J B and Kim Y 2010 Challenges for rechargeable Li batteries *Chem. Mater.* **22** 587–603
[4] Oudenhoven J F M, Baggetto L and Notten P H L 2011 All-solid-state lithium-ion microbatteries: a review of various three-dimensional concepts *Adv. Energy Mater.* **1** 10–33
[5] Bates J B, Dudney N J, Neudecker B, Ueda A and Evans C D 2008 Thin-film lithium and lithium-ion batteries *Solid State Ion.* **135** 33–45
[6] Takada K 2013 Progress and prospective of solid-state lithium batteries *Acta Mater.* **61** 759–70
[7] West W C, Whitacre J F, White V and Ratnakumar B V 2002 Fabrication and testing of all solid-state microscale lithium batteries for microspacecraft applications *J. Micromech. Microeng.* **12** 58–62
[8] Song J, Yang X, Zeng S-S, Cai M-Z, Zhang L-T, Dong Q-F, Zheng M-S, Wu S-T and Wu Q-H 2009 Solid-state microscale lithium batteries prepared with microfabrication processes *J. Micromech. Microeng.* **19** 045004
[9] Zhao S, Fu Z and Qin Q 2002 A solid-state electrolyte lithium phosphorus oxynitride film prepared by pulsed laser deposition *Thin Solid Films* **415** 108–13
[10] Liu J, Banis M N, Li X, Lushington A, Cai M, Li R, Sham T-K and Sun X 2013 Atomic layer deposition of lithium tantalate solid-state electrolytes *J. Phys. Chem.* C **117** 20260–7
[11] Armand M and Tarascon J-M 2008 Building better batteries *Nature* **451** 652–7
[12] Sun K, Wei T-S, Ahn B Y, Seo J Y, Dillon S J and Lewis J A 2013 3D printing of interdigitated Li-ion microbattery architectures *Adv. Mater.* **25** 4539–43
[13] Pikul J H, Gang Zhang H, Cho J, Braun P V and King W P 2013 High-power lithium ion microbatteries from interdigitated three-dimensional bicontinuous nanoporous electrodes *Nat. Commun.* **4** 1732
[14] Joshi R K and Schneider J J 2012 Assembly of one dimensional inorganic nanostructures into functional 2D and 3D architectures. Synthesis, arrangement and functionality *Chem. Soc. Rev.* **41** 5285–312
[15] Meng X, Yang X-Q and Sun X 2012 Emerging applications of atomic layer deposition for lithium-ion battery studies *Adv. Mater.* **24** 3589–615
[16] George S M 2010 Atomic layer deposition: an overview *Chem. Rev.* **110** 111–31
[17] Chen P, Mitsui T, Farmer D B, Golovchenko J, Gordon R G and Branton D 2004 Atomic layer deposition to fine-tune the surface properties and diameters of fabricated nanopores *Nano Lett.* **4** 1333–7
[18] Gordon R G, Hausmann D, Kim E and Shepard J 2003 A kinetic model for step coverage by atomic layer deposition in narrow holes or trenches *Chem. Vapor Depos.* **9** 73–8
[19] Elam J W, Routkevitch D, Mardilovich P P and George S M 2003 Conformal coating on ultrahigh-aspect-ratio nanopores of anodic alumina by atomic layer deposition *Chem. Mater.* **15** 3507–17
[20] Solanki R and Pathangey B 2000 Atomic layer deposition of copper seed layers *Electrochem. Solid-State Lett.* **3** 479–80
[21] Liu J, Tang Y, Xiao B, Sham T-K, Li R and Sun X 2013 Atomic layer deposited aluminium phosphate thin films on N-doped CNTs *RSC Adv.* **3** 4492
[22] Cheah S K, Perre E, Rooth M, Fondell M, Hårsta A, Nyholm L, Boman M, Lu J, Simon P and Edstro K 2009 Self-supported three-dimensional nanoelectrodes for microbattery applications *Nano Lett.* **9** 3230–3
[23] Gerasopoulos K, Chen X, Culver J, Wang C and Ghodssi R 2010 Self-assembled Ni/$TiO_2$ nanocomposite anodes synthesized via electroless plating and atomic layer deposition on biological scaffolds *Chem. Commun. (Camb.)* **46** 7349–51

[24] Gerasopoulos K, Pomerantseva E, Mccarthy M, Brown A, Wang C, Culver J and Ghodssi R 2012 Hierarchical three-dimensional microbattery electrodes combining bottom-up self-assembly and top-down micromachining *ACS Nano* **6** 6422–32

[25] Li X *et al* 2012 Tin oxide with controlled morphology and crystallinity by atomic layer deposition onto graphene nanosheets for enhanced lithium storage *Adv. Funct. Mater.* **22** 1647–54

[26] Kim S, Han T H, Kim J, Gwon H, Moon H, Kang S, Kim S O and Kang K 2009 Fabrication and electrochemical characterization of $TiO_2$ three-dimensional nanonetwork based on peptide assembly *ACS Nano* **3** 1085–90

[27] Meng X, Zhong Y, Sun Y, Banis M N, Li R and Sun X 2011 Nitrogen-doped carbon nanotubes coated by atomic layer deposited $SnO_2$ with controlled morphology and phase *Carbon N. Y.* **49** 1133–44

[28] Badot J C, Mantoux A, Baffier N, Dubrunfaut O, Lincot D and Cedex P 2004 Electrical properties of $V_2O_5$ thin films obtained by atomic layer deposition (ALD) *J. Mater. Chem.* **14** 3411–5

[29] Donders M E, Arnoldbik W M, Knoops H C M, Kessels W M M and Notten P H L 2013 Atomic layer deposition of $LiCoO_2$ thin-film electrodes for all-solid-state Li-ion micro-batteries *J. Electrochem. Soc.* **160** A3066–71

[30] Putkonen M, Aaltonen T, Alnes M, Sajavaara T, Nilsen O and Fjellvåg H 2009 Atomic layer deposition of lithium containing thin films *J. Mater. Chem.* **19** 8767–71

[31] Aaltonen T, Alnes M, Nilsen O, Costelle L and Fjellvåg H 2010 Lanthanum titanate and lithium lanthanum titanate thin films grown by atomic layer deposition *J. Mater. Chem.* **20** 2877–81

[32] Comstock D J and Elam J W 2013 Mechanistic study of lithium aluminum oxide atomic layer deposition *J. Phys. Chem.* C **117** 1677–83

[33] Aaltonen T, Nilsen O, Magras A and Fjellv H 2011 Atomic layer deposition of $Li_2O$–$Al_2O_3$ thin films *Chem. Mater.* **23** 4669–75

[34] Park J S, Meng X, Elam J W, Wolverton C, Kim C and Cabana J 2014 Ultrathin lithium ion conducting coatings for increased interfacial stability in high voltage Li-ion batteries ultrathin lithium ion conducting coatings for increased interfacial stability in high voltage Li-ion batteries *Chem. Mater.* **26** 3128–34

[35] Hämäläinen J, Munnik F, Hatanpää T, Holopainen J, Ritala M and Leskelä M 2012 Study of amorphous lithium silicate thin films grown by atomic layer deposition *J. Vac. Sci. Technol.* A **30** 01A106

[36] Østreng E, Sønsteby H H, Sajavaara T, Nilsen O and Fjellvåg H 2013 Atomic layer deposition of ferroelectric $LiNbO_3$ *J. Mater. Chem.* C **1** 4283–90

[37] Østreng E, Vajeeston P, Nilsen O and Fjellvåg H 2012 Atomic layer deposition of lithium nitride and carbonate using lithium silylamide *RSC Adv.* **2** 6315–22

[38] Perng Y-C, Cho J, Membereno D, Cirigliano N, Dunn B and Chang J P 2014 Synthesis of ion conducting $Li_xAl_ySi_zO$ thin films by atomic layer deposition *J. Mater. Chem.* A doi:10.1039/c3ta14928e

[39] Bates J B, Dudney N J, Gruzalski G R, Zuhr R A and Choudhury A 1993 Fabrication and characterization of amorphous lithium electrolyte thin films and rechargeable thin-film batteries *J. Power Sources* **44** 103–10

[40] Wang B, Chakoumakos B C, Sales B C, Kwak B S and Bates J B 1995 Synthesis, crystal structure, and ionic conductivity of a polycrystalline lithium phosphorus oxygtride with the gamma-$Li_3PO_4$ structrue *J. Solid State Chem.* **115** 313–23

[41] Hamalainen J, Holopainen J, Munnik F, Hatanpaa T, Heikkila M, Ritala M and Leskela M 2012 Lithium phosphate thin films grown by atomic layer deposition *J. Electrochem. Soc.* **159** A259–63

[42] Holopainen J, Munnik F, Heikkila M, Ritala M and Leskela M 2012 Atomic layer deposition of aluminum and titanium phosphates *J. Phys. Chem.* C **116** 5920–5

[43] Appapillai A T, Mansour A N, Cho J and Shao-horn Y 2007 Microstructure of $LiCoO_2$ with and without '$AlPO_4$' nanoparticle coating : combined STEM and XPS studies *Chem. Mater.* **89** 5748–57

[44] Macdonald J R 1992 Impedance spectroscopy *Ann. Biomed. Eng.* **20** 289–305

[45] Martin S W and Angell C A 1986 Dc and ac conductivity in wide composition range $Li_2O$–$P_2O_5$ glasses *J. Non. Cryst. Solids* **83** 185–207

[46] Hu Y W, Raistrick I D and Huggins R A 1997 Ionic conductivity of lithium orthosilicate-lithium phosphate solid solutions *J. Electrochem. Soc.* **124** 1240–2

[47] Sokolov I A, Tarlakov Y P, Ustinov N Y and Pronkin A A 2005 Structure and electric properties of lithium phosphate glasses *Russ. J. Appl. Chem.* **78** 741–6

[48] Li X, Liu J, Banis M N, Lushington A, Li R, Cai M and Sun X 2014 Atomic layer deposition of solid-state electrolyte coated cathode materials with superior high-voltage cycling behavior for lithium ion battery application *Energy Environ. Sci.* **7** 768